Small-Signal Stability Analysis of Low-Inertia Power Grids with Inverter-Based Resources and Synchronous Condensers

Preprint

Lizhi Ding,[1,2] Xiaonan Lu,[2] and Jin Tan[1]

1 National Renewable Energy Laboratory
2 Temple University

To be presented at the 2022 IEEE PES Innovative Smart Grid Technologies Conference (ISGT NA)
February 21–24, 2022

NREL is a national laboratory of the U.S. Department of Energy
Office of Energy Efficiency & Renewable Energy
Operated by the Alliance for Sustainable Energy, LLC

This report is available at no cost from the National Renewable Energy Laboratory (NREL) at www.nrel.gov/publications.

Contract No. DE-AC36-08GO28308

Conference Paper
NREL/CP-5C00-80613
November 2021

Small-Signal Stability Analysis of Low-Inertia Power Grids with Inverter-Based Resources and Synchronous Condensers

Preprint

Lizhi Ding,[1,2] Xiaonan Lu,[2] and Jin Tan[1]

1 National Renewable Energy Laboratory
2 Temple University

Suggested Citation
Ding, Lizhi, Xiaonan Lu, and Jin Tan. 2021. *Small-Signal Stability Analysis of Low-Inertia Power Grids with Inverter-Based Resources and Synchronous Condensers: Preprint*. Golden, CO: National Renewable Energy Laboratory. NREL/CP-5C00-80613.
https://www.nrel.gov/docs/fy22osti/80613.pdf.

NREL is a national laboratory of the U.S. Department of Energy
Office of Energy Efficiency & Renewable Energy
Operated by the Alliance for Sustainable Energy, LLC

This report is available at no cost from the National Renewable Energy Laboratory (NREL) at www.nrel.gov/publications.

Contract No. DE-AC36-08GO28308

Conference Paper
NREL/CP-5C00-80613
November 2021

National Renewable Energy Laboratory
15013 Denver West Parkway
Golden, CO 80401
303-275-3000 • www.nrel.gov

NOTICE

This work was authored in part by the National Renewable Energy Laboratory, operated by Alliance for Sustainable Energy, LLC, for the U.S. Department of Energy (DOE) under Contract No. DE-AC36-08GO28308. Funding provided by U.S. Department of Energy Office of Energy Efficiency and Renewable Energy Solar Energy Technologies Office Award Numbers 34224 and 37772. The views expressed herein do not necessarily represent the views of the DOE or the U.S. Government.

Small-Signal Stability Analysis of Low-Inertia Power Grids with Inverter-Based Resources and Synchronous Condensers

Lizhi Ding[1,2], Student Member, IEEE, Xiaonan Lu[2], Member, IEEE, Jin Tan[1], Member, IEEE
1. Grid Planning and Analysis Center, NREL, Golden, CO, USA 2. College of Engineering, Temple University, Philadelphia, PA, USA

***Abstract*—With the potential environmental impacts of conventional fossil fuels and the technological advances of grid-interactive power electronics, inverter-based resources (IBRs) are playing a crucial role in modern power grids for decarbonization. Several pathways to gradually transition to a 100% renewable power grid are still under discussion, including providing grid inertia by converting the retired synchronous generators into synchronous condensers (SCs) or operating a 100% IBR grid by implementing grid-forming (GFM) inverters. As we move toward 100% renewables, ensuring grid stability is necessary; therefore, understanding the fundamental dynamic stability characteristics of an IBR-dominated grid becomes essential. For this purpose, a generic, small-signal grid model with the detailed control schemes of both SCs and IBRs has been developed. Specifically, the grid-following (GFL) control mode with and without droop control and GFM control mode are modeled separately and compared to understand the main differences and their impact on grid stability in terms of induced oscillation modes and critical control parameters.**

***Index Terms*—Grid-following, grid-forming, low-inertia power grids, modal analysis, small-signal stability, synchronous condenser**

I. Introduction

For environmental and economic reasons, renewable energy is gradually replacing the role of conventional fossil energy and is of increasing significance for future power grids [1]. These renewable resources are usually interfaced with the grid through grid-interactive inverters; however, because of the lack of physical inertia, the impact of grid-connected inverters on power systems is more complex than that of conventional electromagnetic equipment (i.e., synchronous machines and power transformers). Further, with the power grids transitioning toward 100% power-electronics-based power systems, operational instabilities could be triggered; hence, detailed and accurate modeling of power grids with high penetrations of inverter-based resources (IBRs) is needed to address existing and emerging challenges.

Synchronous condensers (SCs), as synchronous machines without prime movers and turbines, can be used as compensatory units to address some operational challenges in power grids with high penetrations of IBRs [2]. With the decreasing inertia of the existing power system and the increasing penetration of IBRs, the entire power system is susceptible to load disturbances; however, SCs, as rotating units, can be used to compensate for the system inertia previously provided by synchronous generators (SGs). This allows additional opportunities for system stability and reliability enhancement.

The existing grid-interactive inverters are generally operated in grid-following (GFL) control mode [3]. The output power or current of GFL inverters is regulated by measuring the phase angle of the grid voltage through dedicated phase-locked loops (PLLs). Although droop control could be developed for GFL inverters to support fast grid frequency regulation, it cannot actively establish grid frequency when transitioning to islanded operation [4]. In contrast, grid-forming (GFM) inverters can actively establish frequency and voltage at the local inverter level, which makes them widely used in microgrids, large-scale distribution systems, and even transmission systems [5].

To ensure that the system is operated safely with a sufficient stability margin, small-signal stability and/or transient stability analyses are usually conducted. This paper investigates the impacts of IBRs with GFL and GFM control on the system in terms of small-signal stability, and it also considers the potential contribution of SCs. Modal analysis is conducted to identify the oscillatory modes of GFL and GFM inverters. Further, the impacts of key parameters (e.g., SC inertia, length of the transmission line) on system stability are also identified.

II. System Modeling

A. Modeling of Synchronous Condensers

In this study, a salient-pole SC is considered. Compared to classic SGs, SCs lack the governor and turbine; thus, they cannot provide active power to the grid.

The voltage equations can be used to describe the dynamics of SCs:

$$\begin{cases} v_{\mathrm{gd}} = -R_{\mathrm{s}} i_{\mathrm{gd}} - \omega_{\mathrm{Gen}} \psi_{\mathrm{gq}} + d\psi_{\mathrm{gd}} / (\omega_{\mathrm{b}} dt) \\ v_{\mathrm{gq}} = -R_{\mathrm{s}} i_{\mathrm{gq}} + \omega_{\mathrm{Gen}} \psi_{\mathrm{gd}} + d\psi_{\mathrm{gq}} / (\omega_{\mathrm{b}} dt) \\ v_{\mathrm{fd}} = R_{\mathrm{fd}} i_{\mathrm{fd}} + d\psi_{\mathrm{fd}} / (\omega_{\mathrm{b}} dt) \\ v_{\mathrm{kq}} = R_{\mathrm{kq}} i_{\mathrm{kq}} + d\psi_{\mathrm{kq}} / (\omega_{\mathrm{b}} dt) \end{cases} \quad (1)$$

where v, i, ψ denote the voltage, current, and flux linkage, respectively; the subscripts $_{\mathrm{d}}$ and $_{\mathrm{q}}$ denote the *d*-axis and *q*-axis; the subscripts $_{\mathrm{gd}}$, $_{\mathrm{gq}}$, $_{\mathrm{fd}}$, and $_{\mathrm{kq}}$ denote the stator *d*-axis, *q*-axis, field circuit, and amortisseur circuit in the *q*-axis, respectively; R_{s}, R_{fd}, and R_{kq} are the equivalent resistance in the stator, field circuit, and amortisseur circuit; ω_{Gen} is the

angular frequency of the SC; and ω_b is the base value. Note that a reciprocal per-unit system is used in this study to simplify the model expression [6].

The relationship between the winding current and the flux linkage is given by the flux linkage equations:

$$\begin{cases} \psi_{gd} = -L_d i_{gd} + L_{ad} i_{fd},\ \psi_{gq} = -L_q i_{gq} + L_{aq} i_{kq} \\ \psi_{fd} = -L_{ad} i_{gd} + L_{fd} i_{fd},\ \psi_{kq} = -L_{aq} i_{gq} + L_{kq} i_{kq} \end{cases} \quad (2)$$

where L_d, L_q, L_{fd}, L_{kq} are the self-inductance; and L_{ad} and L_{aq} are the mutual inductance due to the flux that links the rotor circuits in the *d*-axis and *q*-axis.

The swing equations are used to represent the rotor characteristics:

$$\dot{\delta}_{Gen} = \omega_b(\omega_{Gen} - \omega_{com}),\ 2H\, d\omega_{Gen}/dt + D(\omega_{Gen} - 1) = -T_e \quad (3)$$

where H is the inertia constant; D is the damping coefficient; T_e is the electrical torque; and δ_{Gen} is the phase angle of the SC referring to the common reference frame.

A first-order model is used to represent the field circuit, which is given as:

$$v_{fd} = K_f(v_g^* - v_g)/(1 + sT_f) \quad (4)$$

where T_f is the time constant; K_g is the first-order model gain; and v_g and v_g^* are the SG output voltage and its reference, respectively.

B. Modeling of Grid-Following Inverters

The GFL inverter is configurated to exchange power with the external power grid [7]. The control diagram of the GFL inverter is shown in Fig. 1.

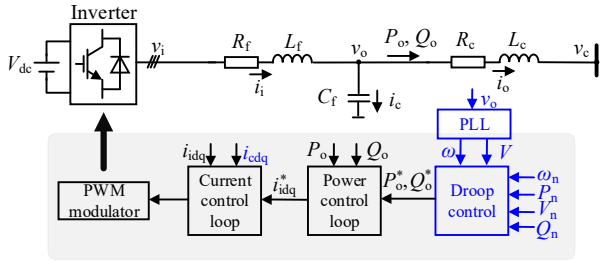

Fig. 1. Block diagram of the GFL inverter control.

The phase angle referring to the common reference frame is given as:

$$\delta_{Inv} = \omega_b \int (\omega_{Inv} - \omega_{com})dt \rightarrow \dot{\delta}_{Inv} = \omega_b(\omega_{Inv} - \omega_{com}) \quad (5)$$

where δ_{Inv} and ω_{Inv} are the inverter phase angle and angular frequency, respectively.

The basic PLL is used to track the frequency, which gives:

$$\dot{\varepsilon}_L = v_{oq} - 0 \quad (6)$$

$$\omega_{Inv} = K_{pL}(v_{oq} - 0) + K_{iL}\varepsilon_L + \omega_n \quad (7)$$

where K_{pL} and K_{iL} are the PI coefficients; and ω_n is the nominal angular frequency and is used here as the feed-forward value.

The low-pass filters (LPFs) are usually used to mitigate the measurement noise, which yields:

$$\dot{P}_{oInv} = -\omega_c P_{oInv} + \omega_c(v_{od} i_{od} + v_{oq} i_{oq}) \quad (8)$$

$$\dot{Q}_{oInv} = -\omega_c Q_{oInv} + \omega_c(v_{oq} i_{od} - v_{od} i_{oq}) \quad (9)$$

where ω_c is the cutoff frequency of the LPFs; and v_{od}, v_{oq}, i_{od}, i_{oq}, P_{oInv}, and Q_{oInv} are the inverter output voltage, current, and power.

When droop control is employed, the GFL control can provide the frequency-watt and/or voltage-var control [2]. Further, when the voltage magnitude is oriented to the *d*-axis, the reference values are given as:

$$P^*_{oInv} = P_{nInv} - (\omega_{Inv} - \omega_n)/m_p,\ Q^*_{oInv} = Q_{nInv} - (v_{od} - V_n)/n_q \quad (10)$$

where m_p, and n_q are the droop coefficients; and P_{nInv}, Q_{nInv}, and V_n are the set points.

For the inner power loop, two intermediate variables, ϕ_d and ϕ_q, are used to model the PI controllers. Thus:

$$\dot{\phi}_d = P^*_{oInv} - P_{oInv},\ \dot{\phi}_q = Q^*_{oInv} - Q_{oInv} \quad (11)$$

$$i^*_{id} = K_{pp}(P^*_{oInv} - P_{oInv}) + K_{ip}\phi_d,\ i^*_{iq} = K_{pq}(Q^*_{oInv} - Q_{oInv}) + K_{iq}\phi_q \quad (12)$$

Meanwhile, for the inner current loop, two intermediate variables, γ_d and γ_q, are used to model the PI controllers. Note that a capacitor-current-feedback loop is used to address the resonance issue introduced by the LCL filter [8]. Thus:

$$\dot{\gamma}_d = i^*_{id} - i_{id},\ \dot{\gamma}_q = i^*_{iq} - i_{iq} \quad (13)$$

$$\begin{cases} v^*_{id} = K_{pc}(i^*_{id} - i_{id}) + K_{ic}\gamma_d - K_v i_{cd} \\ v^*_{iq} = K_{pc}(i^*_{iq} - i_{iq}) + K_{ic}\gamma_q - K_v i_{cq} \end{cases} \quad (14)$$

where K_v is the gain of the capacitor current feedback.

Further, as the interface to connect the inverter and the network, the LCL filter is modeled by assuming that the inverter generates the reference voltage ($v_i = v_i^*$):

$$L_f \dot{i}_{idq} = \omega_b\left(v_{idq} - v_{odq} - R_f i_{idq} \pm \omega_{Inv} L_f i_{iqd}\right) \quad (15)$$

$$C_f \dot{v}_{odq} = \omega_b\left(i_{idq} - i_{odq} \pm \omega_{Inv} C_f v_{oqd}\right) \quad (16)$$

$$L_c \dot{i}_{odq} = \omega_b\left(v_{odq} - v_{cdq} - R_c i_{odq} \pm \omega_{Inv} L_c i_{oqd}\right) \quad (17)$$

C. Modeling of Grid-Forming Inverters

Unlike conventional GFL inverters, GFM inverters, as an emerging solution, can be used to establish the frequency and voltage. Several typical GFM controls can be implemented, such as droop control [9], [10], virtual SG control [11], and virtual oscillator control [12], among others. Because of the simple implementation and autonomous power-sharing characteristics, droop control is widely used and thereby adopted in this study as the sample GFM control [9]. The control diagram of the GFM inverter is shown in Fig. 2.

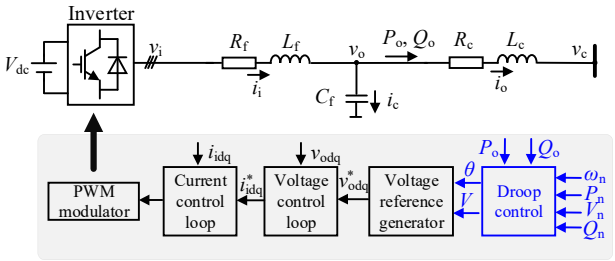

Fig. 2. Block diagram of the GFM inverter control.

When droop control is implemented in GFM inverters and the voltage amplitude is oriented to the *d*-axis, it yields:

$$\omega_{Inv} = \omega_n - m_p(P_{oInv} - P_{nInv}) \quad (18)$$

$$v^*_{od} = V_n - n_q(Q_{oInv} - Q_{nInv}),\ v^*_{oq} = 0 \quad (19)$$

For the inner voltage loop, two intermediate variables, ϕ_d and ϕ_q, are used to model the PI controllers. Thus:

$$\dot{\phi}_d = v^*_{od} - v_{od},\ \dot{\phi}_q = v^*_{oq} - v_{oq} \quad (20)$$

$$i^*_{id} = K_{pv}(v^*_{od} - v_{od}) + K_{iv}\phi_d,\ i^*_{iq} = K_{pv}(v^*_{oq} - v_{oq}) + K_{iv}\phi_q \quad (21)$$

For the modeling of the current loop and LCL filter, it is similar to that of the GFL inverter by merely letting $K_v = 0$ in

the current control loop, and it is not detailed for simplification.

D. Modeling of Networks and Loads

This study uses the constant impedance model for the networks and loads. They should be modeled in the common reference frame to interface with the SC and inverter. Thus:

$$L_t \dot{i}_{tDQ} = \omega_b \left(v_{gDQ} - v_{L2DQ} - R_t i_{tDQ} \pm \omega_{com} L_t i_{tQD} \right) \quad (22)$$

$$L_{L2} \dot{i}_{L2DQ} = \omega_b \left(v_{L2DQ} - R_{L2} i_{L2DQ} \pm \omega_{com} L_{L2} i_{L2QD} \right) \quad (23)$$

where v_{L2DQ} are the bus voltages of the load center.

E. Holistic Modeling of the Entire System

The entire system, as shown in Fig.3, is summarized as:

$$\dot{x} = f(x,u)x + g(x,u)u \quad (24)$$

The small-signal model of the entire system can be obtained by using Lyapunov's first method, and it can be summarized as:

$$\dot{\mathbf{X}}_{sys} = \mathbf{A}_{sys}\mathbf{X}_{sys} \quad (25)$$

where $\mathbf{X}_{sys} = [\Delta\mathbf{X}_{Gen}, \Delta\mathbf{X}_{Inv}, \Delta\mathbf{X}_{Load}, \Delta\mathbf{X}_{Net}]$, $\mathbf{X}_{Gen} = [\omega_{Gen}, \delta_{Gen}, \psi_{gd}, \psi_{gq}, \psi_{fd}, \psi_{kq}, v_{fd}]^T$; $\mathbf{X}_{LoadDQ} = [i_{L2D}, i_{L2Q}]^T$; $\mathbf{X}_{NetDQ} = [i_{tD}, i_{tQ}]^T$; $\Delta\mathbf{X}_{Inv} = [\varepsilon_L, \delta_{Inv}, P_{oInv}, Q_{oInv}, \phi_d, \phi_q, \gamma_d, \gamma_q, i_{id}, i_{iq}, v_{od}, v_{oq}, i_{od}, i_{oq}]^T$ when GFL control is implemented; and $\Delta\mathbf{X}_{Inv} = [\delta_{Inv}, P_{oInv}, Q_{oInv}, \phi_d, \phi_q, \gamma_d, \gamma_q, i_{id}, i_{iq}, v_{od}, v_{oq}, i_{od}, i_{oq}]^T$ when GFM control is implemented.

III. Modal Analysis

A. Test System

Without loss of generality, as shown in Fig.3, one SC unit and one IBR unit are used in this study. The SC is regulated to control the terminal voltage to the rated value. The inverter is configurated in either GFL or GFM operation mode. The load center (i.e., Z_{L2}) is represented by a constant impedance model. Two transmission lines (i.e., Z_t and Z_c) are configured as the network to interface the SC, IBR, and loads.

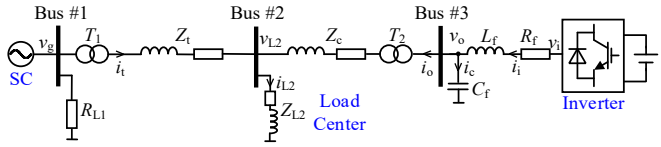

Fig. 3. Test system with one SC and one inverter.

B. Modal Analysis

The eigenvalues can be obtained from (25). The participation factor can be further used to analyze the impacts of the state variables on the corresponding eigenvalues [6]. The oscillatory modes with low real parts are chosen for the analysis. The oscillatory modes are shown in Tables I–III, and the participation factor analyses are summarized in Figs. 4–6.

TABLE I. Oscillatory Modes of GFL Inverter (without Droop) and SC

Eigenvalues	Real	Imag.	Freq.	Damp. Ratio	Type
1, 2 (Mode 1)	-101.29	507.71	80.80	0.20	Coupling
3, 4 (Mode 2)	-129.17	136.14	21.67	0.69	Inverter local
5, 6 (Mode 3)	-32.90	114.89	18.29	0.28	Inverter local
7, 8 (Mode 4)	-1.96	23.31	3.71	0.08	SC local
9, 10 (Mode 5)	-0.97	0.04	0.01	0.99	Inverter local

TABLE II. Oscillatory Modes of GFL Inverter (with Droop) and SC

Eigenvalues	Real	Imag.	Freq.	Damp. Ratio	Type
1, 2 (Mode 1)	-78.81	491.33	78.20	0.16	Coupling
3, 4 (Mode 2)	-107.10	182.09	28.98	0.51	Inverter local
5, 6 (Mode 3)	-92.90	109.55	17.43	0.65	Inverter local
7, 8 (Mode 4)	-2.61	20.47	3.26	0.13	SC local
9, 10 (Mode 6)	-1.29	-3.30	0.52	0.36	Coupling

TABLE III. Oscillatory Modes of GFM Inverter and SC

Eigenvalues	Real	Imag.	Freq.	Damp. Ratio	Type
1, 2 (Mode 1)	-125.68	442.21	70.37	0.27	Coupling
3, 4 (Mode 3)	-35.45	75.61	12.03	0.42	Inverter local
5, 6 (Mode 4)	-1.04	22.71	3.61	0.05	SC local
7, 8 (Mode 7)	-1.79	9.11	1.45	0.19	Coupling
9, 10 (Mode 8)	-0.68	1.03	0.16	0.55	Inverter Local

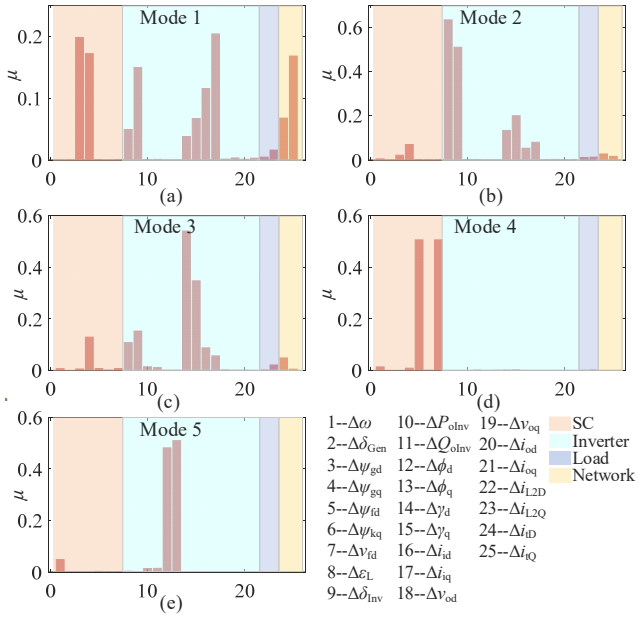

Fig. 4. Participation factor analysis for the GFL inverter without droop. (a) Mode 1. (b) Mode 2. (c) Mode 3. (d) Mode 4. (e) Mode 5.

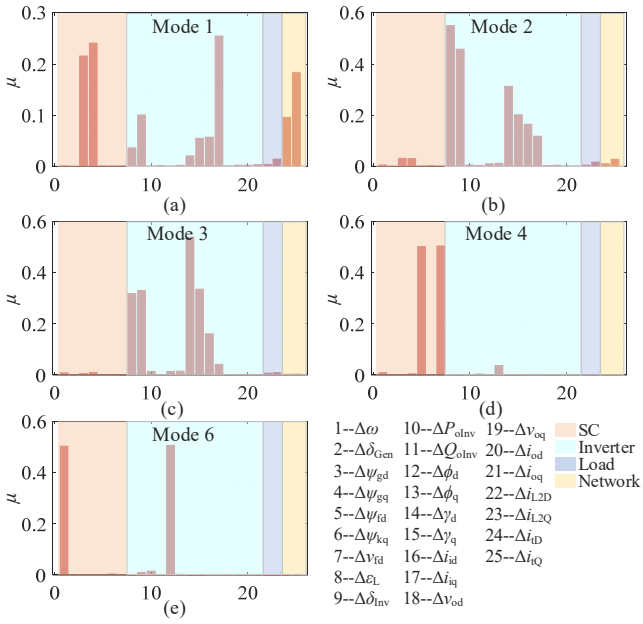

Fig. 5. Participation factor analysis for the GFL inverter with droop. (a) Mode 1. (b) Mode 2. (c) Mode 3. (d) Mode 4. (e) Mode 6.

As shown in Tables I–III and Figs. 4–6, these three controls have similar responses in Mode 1, Mode 3, and Mode 4. Mode 1 is mainly affected by the state variables in the SC, inverter, and network; thus, it is identified as a coupling mode. Mode 3 is mainly affected by the state variables in the inner current loop of the inverter; hence, it is identified as the inverter local mode. Mode 4 is mainly affected by the state variables in the SC field circuit, so it is identified as the SC local mode. Further, the two kinds of GFL inverters (i.e., GFL

without and with outer droop control loop) have a unique mode (i.e., Mode 2), which is generated from the PLL. Further, the GFM inverter also has one unique mode (i.e., Mode 8), which is mainly affected by the voltage loop. As for Mode 5, it is an inverter local model of the GFL inverter without droop because it is merely related to the state variables, ϕ_d, ϕ_q, in the power control. Mode 6 and Mode 7 are the coupling modes for the GFL inverter with droop control and the GFM inverter because the frequency regulation is implemented in these two kinds of inverter control functions.

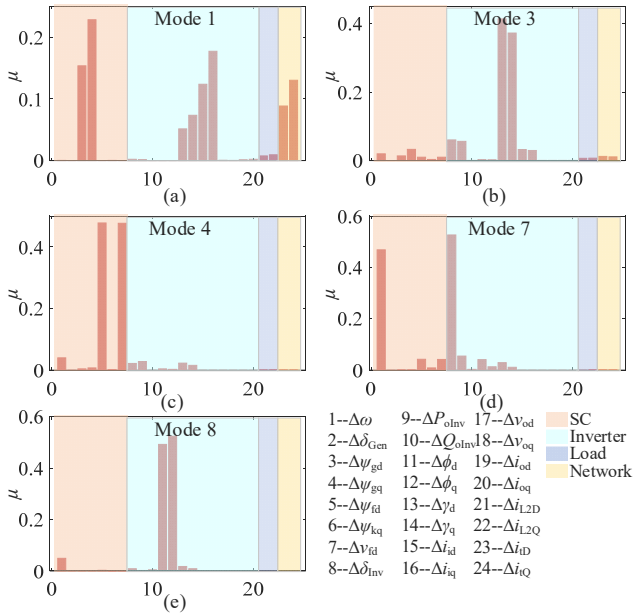

Fig. 6. Participation factor analysis for the GFM inverter. (a) Mode 1. (b) Mode 3. (c) Mode 4. (d) Mode 7. (e) Mode 8.

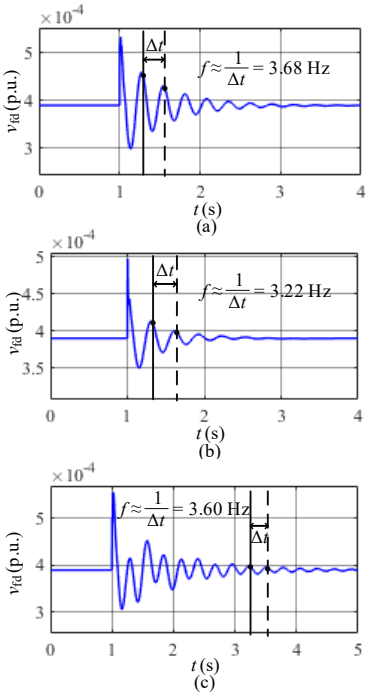

Fig. 7. Time-domain waveforms of the field voltage after a small load disturbance. (a) GFL inverter without droop. (b) GFL inverter with droop. (c) GFM inverter.

C. *Time-Domain Verification*

The time-domain waveforms are provided to verify the modal analysis. An impedance load disturbance is applied at t = 1 s. The SC field voltage is chosen to conduct the verification analysis. As shown in Fig. 7 (a), the measured signal from the GFL inverter without droop configuration contains a 3.68-Hz mode, which corresponds to Mode 4 with the damped frequency of 3.71 Hz in Table I with a small error. A similar observation can be obtained by comparing the results in Fig. 7 (b) and Mode 4 in Table II, Fig. 7 (c) and Mode 4 in Table III.

IV. Impact of Key Parameters

This section studies the impacts of key parameters (i.e., SC inertia, transmission line length) on system stability. The eigenvalue trajectory plots related to the oscillatory modes are obtained accordingly. The baseline values used in this study are given in Table IV.

TABLE IV. Baseline Values

Variable	Value	Unit
Inertia constant, H	0.74	s
SC-side transmission line length	50	km

A. *Impact of Inertia*

The SC inertia is decreased from 100% to 1% of the baseline value. As shown in Figs. 8-10, the system can ensure stable operation within the given range but tends to be unstable. Further, the dominant mode of GFL inverter without droop and with droop (i.e., Mode 4) is different from the dominant mode of GFM inverter (i.e., Mode 7), which indicates different coupling mechanisms between inverter and SC under GFL and GFM control scenarios.

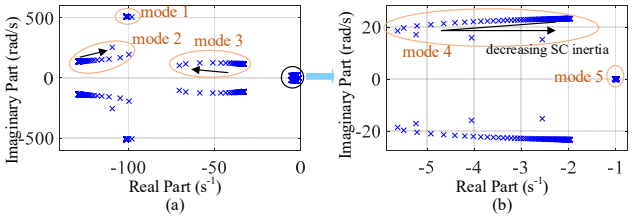

Fig. 8. Eigenvalue trajectory plots showing the (a) impact of the SC inertia on the GFL inverters without droop control. (b) Zoom-in results.

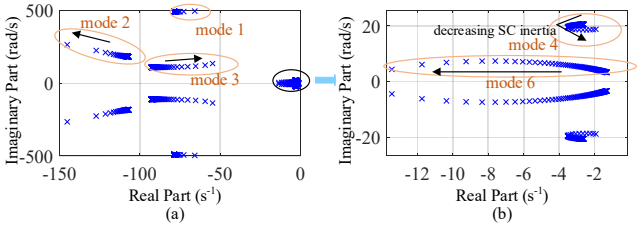

Fig. 9. Eigenvalue trajectory plots showing the (a) impact of the SC inertia on the GFL inverters with droop control. (b) Zoom-in results.

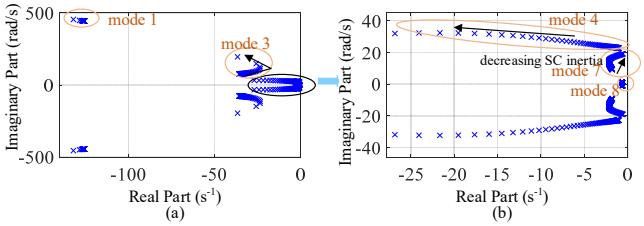

Fig. 10. Eigenvalue trajectory plots showing (a) impact of SC inertia on GFM inverters. (b) Zoom-in results.

B. *Impact of Transmission Line Length*

The length of the SC-side transmission line was changed from 50 km to 500 km. As shown in Figs. 11–13, the shorter transmission line will usually ensure stable operation and enough stability margin. Further, it is observed that the dominant modes of these three control functions are different, which further indicates the different mechanisms among these three control algorithms.

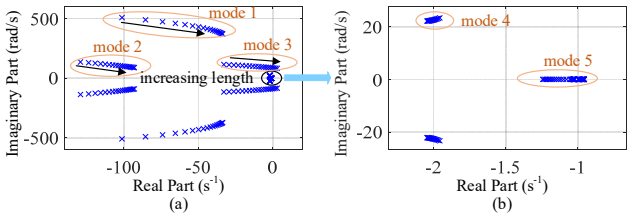

Fig. 11. Eigenvalue trajectory plots showing the (a) impact of the transmission line length on the GFL inverter without droop control. (b) Zoom-in results.

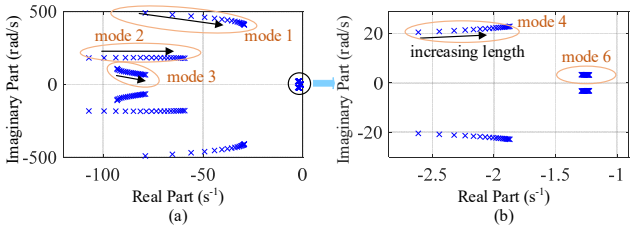

Fig. 12. Eigenvalue trajectory plots showing the (a) impact of the transmission line length on the GFL inverter with droop control. (b) Zoom-in results.

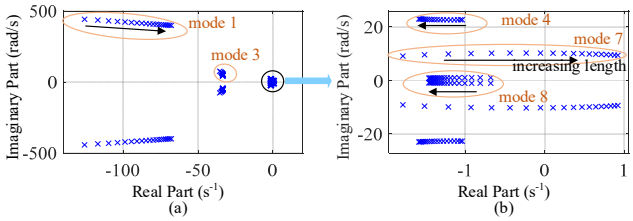

Fig. 13. Eigenvalue trajectory plots showing the (a) impact of the transmission line length on the GFM inverter. (b) Zoom-in results.

V. Conclusion

The small-signal stability analysis of one SC unit and one inverter with either GFL or GFM control was conducted. The analysis showed that there is an additional coupling mode between the inverter and the SC if droop control is implemented in either GFL control with an outer droop control loop or GFM control. Based on the modal analysis, the impacts of the SC inertia and the length of the transmission line on system stability were conducted. The results show that the lack of physical inertia could pose stability issues in inverters. The transmission line length also affects system stability. It is found that the shorter transmission line enhances the system small-signal stability.

Note that the system's complexity will increase if a large number of SCs and inverters are considered; however, this is not the focus of this study because we want to contribute to the basic coupling mechanism between SCs and inverters, which can help system operators gradually increase the penetration of renewable resources without triggering severe instability. Future work will focus on transient stability analysis and large-scale systems to obtain a complete understating of the power network with both IBRs and SCs.

Acknowledgments

This work was authored in part by the National Renewable Energy Laboratory, operated by Alliance for Sustainable Energy, LLC, for the U.S. Department of Energy (DOE) under Contract No. DE-AC36-08GO28308. Funding provided by U.S. Department of Energy Office of Energy Efficiency and Renewable Energy Solar Energy Technologies Office Award Numbers 34224 and 37772. The views expressed in the article do not necessarily represent the views of the DOE or the U.S. Government. The U.S. Government retains and the publisher, by accepting the article for publication, acknowledges that the U.S. Government retains a nonexclusive, paid-up, irrevocable, worldwide license to publish or reproduce the published form of this work, or allow others to do so, for U.S. Government purposes.

References

[1] U. Markovic, O. Stanojev, P. Aristidou, E. Vrettos, D. Callaway, and G. Hug, "Understanding small-signal stability of low-inertia systems," *IEEE Transactions on Power Systems*, vol. 36, no. 5, pp. 3997–4017, Sep. 2021.

[2] R. W. Kenyon, A. Hoke, J. Tan, and B.-M. Hodge, "Grid-following inverters and synchronous condensers: a grid-forming pair?," in *2020 Clemson University Power Systems Conference (PSC)*, Mar. 2020, pp. 1–7.

[3] W. Du et al., "Modeling of grid-forming and grid-following inverters for dynamic simulation of large-scale distribution systems," *IEEE Transactions on Power Delivery*, vol. 36, no. 4, pp. 2035–2045, Aug. 2021.

[4] D. Pattabiraman, R. H. Lasseter., and T. M. Jahns, "Comparison of grid following and grid forming control for a high inverter penetration power system," in *2018 IEEE Power Energy Society General Meeting (PESGM)*, Aug. 2018, pp. 1–5.

[5] R. Rosso, X. Wang, M. Liserre, X. Lu, and S. Engelken, "Grid-forming converters: control approaches, grid-synchronization, and future trends—a review," *IEEE Open Journal of Industry Applications*, vol. 2, pp. 93–109, 2021.

[6] P. Kundur, Power System Stability and Control (ser. The EPRI Power System Engineering). Palo Alto, CA, USA: McGraw-Hill, 1994.

[7] L. Ding et al., "Region-based stability analysis of resilient distribution systems with hybrid grid-forming and grid-following inverters," in *2020 IEEE Energy Conversion Congress and Exposition (ECCE)*, Oct. 2020, pp. 3733–3740.

[8] D. Pan, X. Ruan, C. Bao, W. Li, and X. Wang, "Capacitor-current-feedback active damping with reduced computation delay for improving robustness of LCL-type grid-connected inverter," *IEEE Transactions on Power Electronics*, vol. 29, no. 7, pp. 3414–3427, Jul. 2014.

[9] N. Pogaku, M. Prodanovic, and T. C. Green, "Modeling, analysis and testing of autonomous operation of an inverter-based microgrid," *IEEE Transactions on Power Electronics*, vol. 22, no. 2, pp. 613–625, Mar. 2007.

[10] Y. Du, X. Lu, H. Tu, J. Wang, and S. Lukic, "Dynamic microgrids with self-organized grid-forming inverters in unbalanced distribution feeders," *IEEE Journal of Emerging and Selected Topics in Power Electronics*, vol. 8, no. 2, pp. 1097–1107, Jun. 2020.

[11] Q.-C. Zhong and G. Weiss, "Synchronverters: inverters that mimic synchronous generators," *IEEE Transactions on Industrial Electronics*, vol. 58, no. 4, pp. 1259–1267, Apr. 2011.

[12] B. B. Johnson, S. V. Dhople, A. O. Hamadeh and P. T. Krein, "Synchronization of parallel single-phase inverters with virtual oscillator control," *IEEE Transactions on Power Electronics*, vol. 29, no. 11, pp. 6124-6138, Nov. 2014.